Structural basis for membrane recruitment and allosteric activation of cytohesin family Arf GTPase exchange factors

Andrew W. Malaby, Bert van den Berg[1], and David G. Lambright[2]

Program in Molecular Medicine and Department of Biochemistry and Molecular Pharmacology, University of Massachusetts Medical School, Worcester, MA 01605

Edited by John Kuriyan, University of California, Berkeley, CA, and approved July 23, 2013 (received for review January 29, 2013)

Membrane recruitment of cytohesin family Arf guanine nucleotide exchange factors depends on interactions with phosphoinositides and active Arf GTPases that, in turn, relieve autoinhibition of the catalytic Sec7 domain through an unknown structural mechanism. Here, we show that Arf6-GTP relieves autoinhibition by binding to an allosteric site that includes the autoinhibitory elements in addition to the PH domain. The crystal structure of a cytohesin-3 construct encompassing the allosteric site in complex with the head group of phosphatidyl inositol 3,4,5-trisphosphate and N-terminally truncated Arf6-GTP reveals a large conformational rearrangement, whereby autoinhibition can be relieved by competitive sequestration of the autoinhibitory elements in grooves at the Arf6/PH domain interface. Disposition of the known membrane targeting determinants on a common surface is compatible with multivalent membrane docking and subsequent activation of Arf substrates, suggesting a plausible model through which membrane recruitment and allosteric activation could be structurally integrated.

Guanine nucleotide exchange factors (GEFs) activate GTPases by catalyzing exchange of GDP for GTP (1). Because many GEFs are recruited to membranes through interactions with phospholipids, active GTPases, or other membrane-associated proteins (1–5), GTPase activation can be restricted or amplified by spatial–temporal overlap of GEFs with binding partners. GEF activity can also be controlled by autoregulatory mechanisms, which may depend on membrane recruitment (6–11). Structural relationships between these mechanisms are poorly understood.

Arf GTPases function in trafficking and cytoskeletal dynamics (5, 12, 13). Membrane partitioning of a myristoylated (myr) N-terminal amphipathic helix primes Arfs for activation by Sec7 domain GEFs (14–17). Cytohesins comprise a metazoan Arf GEF family that includes the mammalian proteins cytohesin-1 (Cyth1), ARNO (Cyth2), and Grp1 (Cyth3). The *Drosophila* homolog *steppke* functions in insulin-like growth factor signaling, whereas Cyth1 and Grp1 have been implicated in insulin signaling and Glut4 trafficking, respectively (18–20). Cytohesins share a modular architecture consisting of heptad repeats, a Sec7 domain with exchange activity for Arf1 and Arf6, a PH domain that binds phosphatidyl inositol (PI) polyphosphates, and a C-terminal helix (CtH) that overlaps with a polybasic region (PBR) (21–28). The overlapping CtH and PBR will be referred to as the CtH/PBR. The phosphoinositide specificity of the PH domain is influenced by alternative splicing, which generates diglycine (2G) and triglycine (3G) variants differing by insertion of a glycine residue in the β1/β2 loop (29). Despite similar $PI(4,5)P_2$ (PIP_2) affinities, the 2G variant has 30-fold higher affinity for $PI(3,4,5)P_3$ (PIP_3) (30). In both cases, PIP_3 is required for plasma membrane (PM) recruitment (23, 26, 31–33), which is promoted by expression of constitutively active Arf6 or Arl4d and impaired by PH domain mutations that disrupt PIP_3 or Arf6 binding, or by CtH/PBR mutations (8, 34–36).

Cytohesins are autoinhibited by the Sec7-PH linker and CtH/PBR, which obstruct substrate binding (8). Autoinhibition can be relieved by Arf6-GTP binding in the presence of the PIP_3 head group (8). Active myr-Arf1 and myr-Arf6 also stimulate exchange activity on PIP_2-containing liposomes (37). Whether this effect is due to relief of autoinhibition per se or enhanced membrane recruitment is not yet clear. Phosphoinositide recognition by PH domains, catalysis of nucleotide exchange by Sec7 domains, and autoinhibition in cytohesins are well characterized (8, 16, 17, 30, 38–43). How Arf-GTP binding relieves autoinhibition and promotes membrane recruitment is unknown. Here, we determine the structural basis for relief of autoinhibition and investigate potential mechanistic relationships between allosteric regulation, phosphoinositide binding, and membrane targeting.

Results

Arf6-GTP Binding Requires Autoinhibitory and Membrane Targeting Elements. Although necessary, it is not known whether the PH domain is sufficient for Arf6-GTP binding or whether the N-terminal helix of Arf6 contributes. To delineate the structural requirements, exchange and surface plasmon resonance (SPR) experiments were performed in the presence of $Ins(1,3,4,5)P_4$ (IP_4) to quantify interaction of Grp1 deletion constructs with constitutively active (Q67L) variants of full-length Arf6 or a truncated construct lacking the N-terminal helix (Arf6NΔ13). Both Arf6 constructs had similar stimulatory effects on Grp1 exchange activity (Fig. 1 *A* and *B*), with half-maximal constants ($K_{0.5}$ = 18 μM) similar to the value of 14 μM for Arf6-GppNHp (8). As shown in Fig. 1*C*, Arf6 Q67L bound $Grp1_{251–399}$, which contains the entire linker and CtH/PBR, with an equivalent dissociation constant (K_D = 17 μM). Comparable dissociation constants were observed for constructs truncating up to 10 residues in the linker region (Fig. 1 *D* and *E*). Affinity was reduced fourfold by deletion of the entire linker, twofold by deletion of two residues at the C terminus, and was strongly impaired by deletion of the CtH/PBR (K_D > 200 μM). The minimal construct with intact affinity, $Grp1_{260–399}$, includes the CtH/PBR and five residues from the linker. Conversely, full-length and N-terminally truncated Arf6 Q67L bound $Grp1_{251–399}$ with indistinguishable K_D values of 16–18 μM.

Author contributions: A.W.M. and D.G.L. designed research; A.W.M. and B.v.d.B. performed research; A.W.M. contributed new reagents/analytic tools; A.W.M. and D.G.L. analyzed data; and A.W.M., B.v.d.B., and D.G.L. wrote the paper.

The authors declare no conflict of interest.

This article is a PNAS Direct Submission.

Data deposition: The atomic coordinates have been deposited in the Protein Data Bank, www.pdb.org (PDB ID code 4KAX).

[1]Present address: Institute for Cell and Molecular Biosciences, Medical School, Newcastle University, Newcastle upon Tyne NE2 4HH, England.

[2]To whom correspondence should be addressed. E-mail: david.lambright@umassmed.edu.

This article contains supporting information online at www.pnas.org/lookup/suppl/doi:10.1073/pnas.1301883110/-/DCSupplemental.

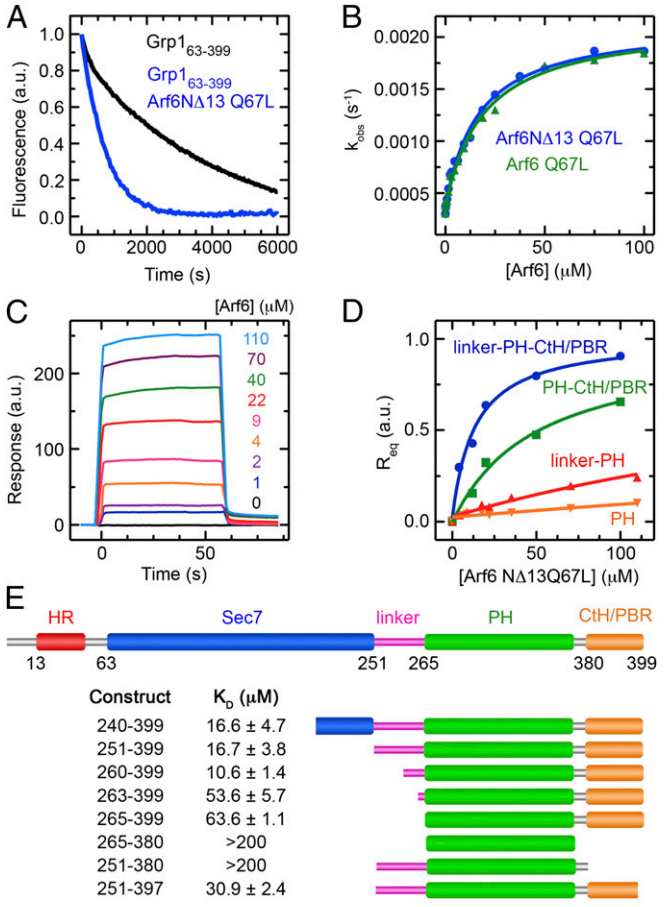

Fig. 1. Structural requirements for Arf6-GTP binding and relief of autoinhibition. (*A*) MantGDP dissociation from Arf1NΔ17 catalyzed by 125 nM $Grp1_{63–399}$ in the presence or absence of 80 μM Arf6NΔ13 Q67L. (*B*) Dependence $Grp1_{63–399}$ catalyzed mantGDP dissociation from Arf1NΔ17 on Arf6 Q67L or Arf6NΔ13 Q67L. (*C*) SPR sensorgrams for binding of 6×His Arf6NΔ13 Q67L to immobilized GST-$Grp1_{251–399}$. (*D*) Dependence of equilibrium SPR signals (R_{eq}) for selected Grp1 constructs on Arf6NΔ13 Q67L. (*E*) Dissociation constants for 6×His Arf6NΔ13 Q67L binding to GST-Grp1 constructs determined by SPR. All buffers contained 1 μM IP_4.

Structure of the Arf6–GTP Complex with Grp1-IP_4. Crystals diffracting to 1.8 Å were obtained for Arf6NΔ13 Q67L bound to $Grp1_{247–399}$ and IP_4. The structure was solved by molecular replacement (*Materials and Methods*, Table S1, and Fig. S1). The structures of Arf6-GTP and the PH domain resemble those of the isolated proteins, as do the interactions with bound ligands (39, 40, 44). As illustrated in Fig. 2 and Fig. S2, the complex buries a surface area of 2,450 $Å^2$ within a tripartite interface that includes intermolecular interactions with the PH domain as well as intermolecular and intramolecular interactions involving the linker and CtH/PBR. At the core of the PH domain interface (Fig. 2*B*), the β1 strand, switch II, and interswitch regions of Arf6 engage the extended sheet comprised of the β1–β4 strands and βi1–βi2 hairpin insertion in the PH domain. Notably, the βi1–βi2 hairpin is a unique feature of cytohesins and supplies basic residues critical for phosphoinositide recognition (39, 40). Invariant Arf6 residues from switch I (Phe-47), interswitch (Trp-62), and switch II (Leu-73, His-76, and Tyr-77) pack against nonpolar residues from the β3–β4 strands (Cys-292, Tyr-294, Ile-307, and Pro-309) and βi1–βi2 hairpin (Cys-342 and Val-350) in the PH domain. At the periphery, interswitch (Asn-48) and switch II (Lys-69) residues mediate polar interactions with, respectively, residues from the β6-βi1 (Lys-340) and β2–β3 (Asp-290) loops in the PH domain. Arg-15 in the β1 strand of Arf6 also donates a hydrogen bond to the main chain carbonyl of Val-350 in the βi2 strand of the PH domain. Despite differences in detail, the PH domain interaction epitope in Arf6 is centered on the invariant hydrophobic triad at the switch/interswitch junction (Fig. S3*A*) and, in this respect, resembles previously described Arf–effector complexes (45). The interaction epitope in the PH domain, on the other hand, is distinct from GTPase interaction epitopes in other PH domain complexes, including Arf1-GTP/ARHGAP21 (Fig. S3*B*) (46).

The interface of canonical Arf and noncanonical PH domain surfaces facilitates an unusual mode of interaction with the linker and CtH/PBR. The CtH, including the first two residues of the PBR, and the last nine residues in the linker dock in distinct grooves formed at the periphery of the central Arf6-PH domain interface (Fig. 2 *C* and *D*). In one groove, Leu-258 and Phe-262 in the linker occupy hydrophobic pockets derived from switch II residues (Pro-72, Leu-73, Arg-75, and His-76) and the PH domain β3/β4 loop (Ile-287, Tyr-294, Phe-296, and Lys-307). In the other groove, Phe-384, Leu-388, and Lys-392 from the CtH/PBR pack against a concave surface lined by switch I (Tyr-31) and interswitch (Thr-40 and Ile-42) residues. Whereas the interactions with the CtH/PBR are mediated primarily by Arf6 residues, the linker contacts are more evenly distributed between Arf6 and the PH domain. These observations explain the stronger reduction in affinity accompanying deletion of the CtH/PBR compared with deletion of the linker, despite similar buried surface areas (757 $Å^2$ vs. 648 $Å^2$, respectively).

Structural Basis for Relief of Autoinhibition by Arf6-GTP. Comparison of the active Arf6-Grp1 and autoinhibited Grp1 structures after

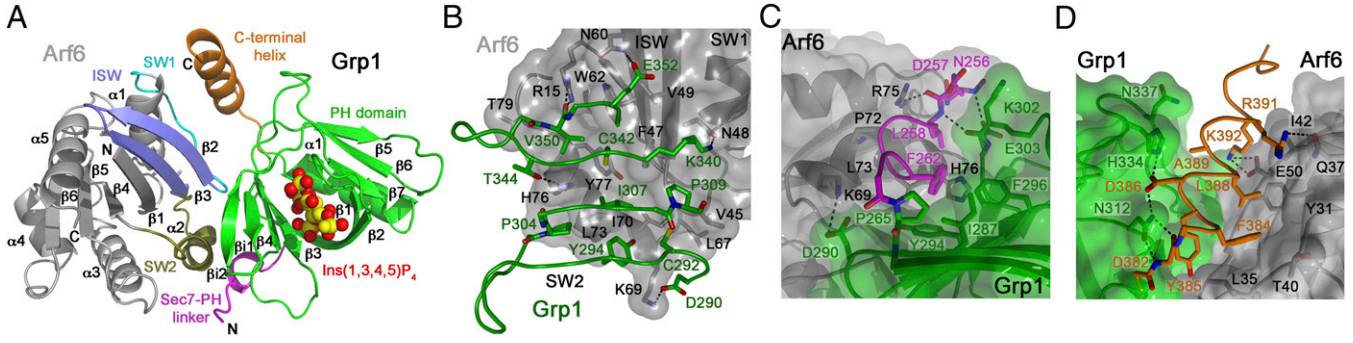

Fig. 2. Structure of Arf6NΔ13 Q67L in complex with $Grp1_{247–399}$ and IP_4. (*A*) Overall view of the complex with the switch (SW), interswitch (ISW), and other regions colored as indicated. IP_4 is depicted as spheres. (*B*) Core interface between Arf6 and the Grp1 PH domain. (*C* and *D*) Docking of the linker (*C*) and CtH/PBR (*D*) within grooves at the periphery of the Arf6-PH domain interface. Molecules and relevant regions are colored as indicated in *A*.

superposition of the PH domain reveals large conformational rearrangements in which the linker rotates ~120° about Asp-266 at linker/PH domain junction, whereas the CtH/PBR rotates ~90° about Ser-378 and Ile-379 in the turn preceding the CtH (Fig. 3 and Movie S1). The linker rotation is accompanied by changes in its irregular secondary structure. Moreover, several residues that occupy the Sec7 domain exchange site in the autoinhibited structure, including Leu-258 in the linker and Phe-384, Leu-388, and Lys-392 in the CtH/PBR, are buried in the grooves formed at the Arf6-PH domain interface (Fig. S2). Thus, Arf6-GTP binding relieves autoinhibition through an allosteric mechanism involving competitive sequestration of the linker and CtH/PBR in conformations incompatible with autoinhibition. Consistent with these observations, the L388A and K392A substitutions in the CtH/PBR strongly reduce Arf6-GTP binding (Fig. 4*A*), explaining why these mutations disrupt insulin-stimulated PM recruitment (8).

Determinants of Activation and Arf-GTP Recognition. The I307E and K340A mutations in the Grp1 PH domain interfere with Arf6-dependent cell spreading and PM recruitment (34, 47). The equivalent K336A mutation in ARNO impairs myr-Arf6-GTP stimulation of GEF activity for myr-Arf1 on liposomes containing PIP_2 (37). Lys-340 mediates a polar interaction with Asn-48 in the interswitch region (Fig. 2*B*), whereas Ile-307 is buried in a pocket formed by the hydrophobic triad (Fig. S3*A*) and conforms to a common theme in Arf:effector recognition (45). To further explore the significance of the structural observations and identify determinants for activation by Arf6-GTP, residues in the interface were mutated and the effects quantified by measuring the catalytic efficiency (k_{cat}/K_M) for Arf1NΔ17-mantGDP/GppNHp exchange in the presence or absence of 80 μM Arf6NΔ13 Q67L. This concentration is fourfold greater than $K_{0.5}$ for activation and affords robust stimulation while maintaining sensitivity to changes in k_{cat}/K_M. Arf6NΔ13 Q67L increased k_{cat}/K_M 11-fold, which was moderately to severely impaired by switch I (F47A) or switch II (H76A) substitutions (Fig. 4*B* and Table S2). PH domain substitutions (Y294A in β3, I307A or I307E in β4, K340A in the β6-βi1 loop, or V350A in βi2) also rendered Grp1 refractory to activation. Finally, alanine substitution of the terminal 2–3 residues in the PBR disrupted autoinhibition and, consequently, activation by Arf6NΔ13 Q67L. Although disordered in the autoinhibited Grp1 structure, the C-terminal lysine residues may contribute to the stability of the CtH through electrostatic interaction with the helix dipole.

To clarify the specificity for active Arf GTPases, relief of autoinhibition by the five human Arf family members was examined (Fig. S4). Compared with Arf6NΔ13 Q67L, stimulation by the N-terminally truncated forms of other Arf GTPases was weaker (two- to fourfold). Assuming the extent of activation is similar at saturation, two- to fourfold stimulation is consistent with $K_{0.5}$ values that are 10- to 25-fold lower than that for Arf6. Given similar tertiary structures, the preference for Arf6 might reflect nonconservative substitutions in the binding interface. Similarity within the interaction epitope (Fig. S4*A*) suggested five putative specificity determinants. Individual mutation of these residues in Arf1 and Arf6 resulted in reciprocal perturbations of twofold or less (Fig. S4*B*). The combination of all five substitutions in Arf1 had little additional effect, as was the case for an Arf1→6 chimera that included the complete set of 10 substitutions in the binding epitope. Thus, whereas the specificity for some effectors can be reversed by interfacial substitutions in the switch/interswitch regions (48), the interaction with Grp1 is also sensitive to determinants outside the binding epitope.

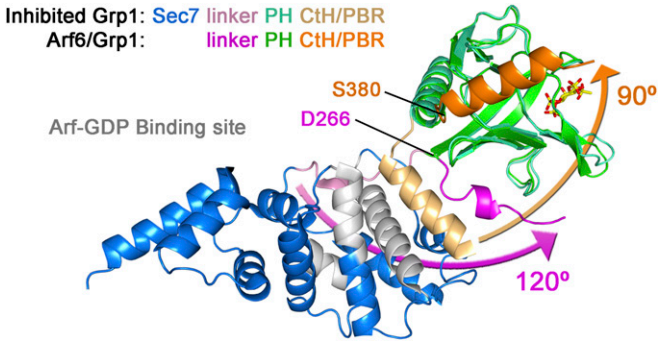

Fig. 3. Structural basis for relief of autoinhibition by Arf6. Comparison of autoinhibited Grp1 (PDB ID code 2R09) with the active Arf6 complex after superposition of the PH domains. Arrows indicate the angular displacement of the linker and CtH/PBR.

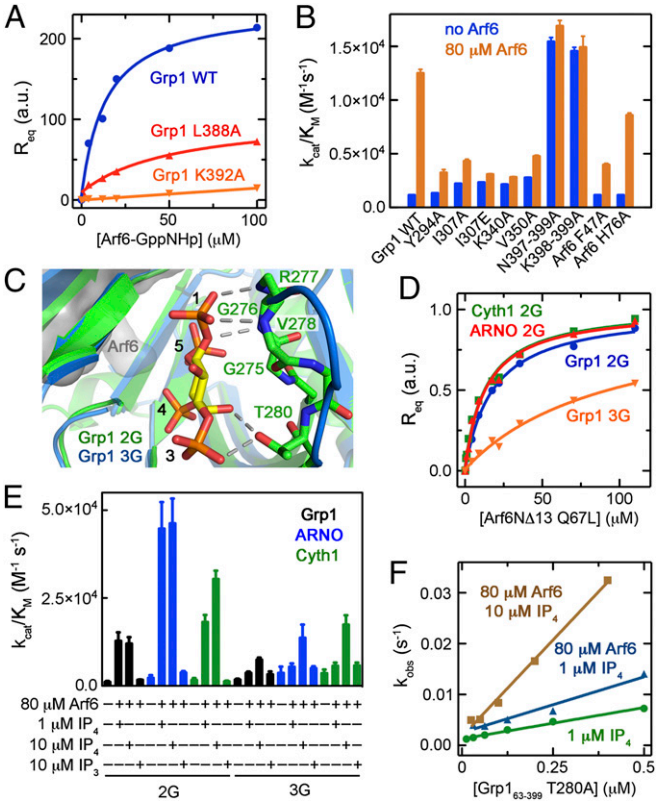

Fig. 4. Structure-based mutational analysis of Arf6-GTP binding and relief of autoinhibition. (*A*) Effect of mutations in the CtH/PBR of GST-$Grp1_{251–399}$ on R_{eq} as a function of 6×His Arf6NΔ13-GppNHp in buffer containing 1 μM IP_4. Curves are fitted models. (*B*) Effect of mutations on the k_{cat}/K_M of $Grp1_{63–399}$ for Arf1NΔ17 in buffer containing 1 μM IP_4 with or without 80 μM Arf6NΔ13 Q67L. (*C*) Comparison of head group binding sites in the 2G Grp1 PH domain from the Arf6 complex and the 3G Grp1 PH domain bound to IP_4 (PDB ID code 1U2B) after superposition. (*D*) R_{eq} for 6×His Arf6NΔ13 Q67L binding to 2G GST-$Grp1_{251–399}$, 3G GST-$Grp1_{251–399}$, 2G $ARNO_{247–397}$, and 2G GST-$Cyth1_{251–399}$. Curves are fitted models. (*E*) Effect of 2G vs. 3G splice variation on the k_{cat}/K_M of $Grp1_{63–399/400}$, $ARNO_{57–397/398}$, and $Cyth1_{57–399/400}$ for Arf1NΔ17-mantGDP in the presence or absence of IP_4, IP_3, and/or Arf6NΔ13 Q67L. (*F*) Effect of IP_4 on catalysis of mantGDP release from Arf1NΔ17 as a function of $Grp1_{63–399}$ T280A. Lines are linear fits.

Relationship Between Phosphoinositide and Arf6-GTP Binding. The IP_4 requirement is a striking property of Arf6-GTP binding and relief of autoinhibition (8, 34). The underlying structural basis may be related to conformational changes in the βi1/βi2 hairpin and β3/β4 loop, which mediate key contacts with both the head

group and Arf6-GTP. Indeed, subtle structural differences in these elements have been described for IP_4 binding to the Grp1 PH domain (40). Head group binding may also overcome an electrostatic barrier resulting from proximity of the electropositive PBR and head group site in the Arf6–GTP complex.

Substantially higher Arf6-GTP concentrations are required to stimulate 3G ARNO or 3G Cyth1 compared with the 2G variants (8). Because the residues in the Arf6-GTP binding epitope are conserved and the β1/β2 loop containing the splice site is located distal to the interface (Fig. 4*C*), the differences in stimulation are likely an indirect effect of reduced affinity of the 3G variants for IP_4 (30). Consistent with this prediction, the 2G variants bound Arf6NΔ13 Q67L with comparable affinity (Fig. 4*D*) and were robustly stimulated by Arf6NΔ13 Q67L (Fig. 4*E* and Table S3). The 3G variants, however, exhibited muted stimulation that was enhanced by increasing the IP_4 concentration. Similar results were obtained for the T280A mutation in the β1/β2 loop (Fig. 4*F*), which eliminates polar interactions with the 1-phosphate (Fig. 4*C*) and reduces the affinity for IP_4 by 13-fold (30). Replacing IP_4 with Ins(1,4,5)P_3 (IP_3) also substantially diminished Arf6NΔ13 Q67L stimulation.

Relief of Autoinhibition in a Membrane Environment. Membrane partitioning of cytohesins and myristoylated Arfs results in high local concentrations within the restricted volume proximal to the membrane surface. Because binding of myr-Arf-GTP can enhance membrane recruitment and because the product of the exchange reaction is also a potential activator/recruiter, experiments analyzing relief of autoinhibition on membranes must distinguish allosteric activation from restricted volume effects and feedback amplification (37). Thus, Arf1NΔ17-mantGDP was used as a nonpartitioning substrate reporter for the autoinhibitory status of 2G Grp1 in the presence and absence of myr-Arf6 Q67L or Arf6NΔ13 Q67L and liposomes with or without PIP_3 or PIP_2 (Fig. 5 *A*–*C*). Under the conditions of these experiments, the fraction of Grp1 partitioned with membranes in the absence of myr-Arf6 Q67L is >60% for large unilamelar vesicles (LUVs) containing PIP_3 and <10% for LUVs containing either 3 mol % PIP_2 or no phosphoinositide (Fig. S5). As shown in Fig. 5*B*, the exchange activity of Grp1 increased substantially with increasing concentrations of myr-Arf6 Q67L in the presence of liposomes containing PIP_3 ($K_{0.5}$ ~ 75 nM), whereas weaker stimulation was observed in the presence of liposomes containing PIP_2 ($K_{0.5}$ ~ 350 nM) or no phosphoinositide ($K_{0.5}$ ~ 800 nM). Truncation of the Arf6 N terminus increased $K_{0.5}$ by two to three orders of magnitude, whereas the K340A mutation in the PH domain, which disrupts Arf6-GTP binding, eliminated the stimulatory effect (Fig. 5*C*). Similar stimulation was observed for 2G ARNO in the presence of liposomes containing PIP_3 (Fig. S6).

When experiments were performed with myr-Arf1-mantGDP as the substrate and myr-Arf6 Q67L as the activating GTPase (Fig. 5 *D*–*F*), strong stimulation was observed in the presence of PIP_3 ($K_{0.5}$ ~ 50 nM), moderate stimulation in the presence of PIP_2 ($K_{0.5}$ ~ 170 nM), and weaker stimulation in the absence of phosphoinositide ($K_{0.5}$ ~ 330 nM). Substantially weaker stimulation in the presence PIP_3 was observed for myr-Arf1 Q71L (Fig. S4*C*; $K_{0.5}$ ~ 1,200 nM) as well as the Grp1 I307E mutant (Fig. 5*F*; $K_{0.5}$ ~ 1,600 nM). Although the experiments combining myristoylated substrate and activator GTPases do not distinguish membrane recruitment from allosteric activation per se, the overall trends are consistent with the experiments using truncated substrate and myristoylated activator and the experiments with truncated substrate and activator GTPases in the absence of membranes.

Discussion

We have shown that high-affinity Arf6-GTP binding to Grp1 requires the proximal elements implicated in autoinhibition and/or membrane targeting. The structure of the complex revealed an unusual binding modality whereby formation of the Arf6-GTP/PH domain interface creates grooves that sequester the linker and CtH/PBR. Substitutions within the binding interface contribute substantially to the observed specificity but do not fully explain the preference for Arf6. Grp1 engages common Arf recognition determinants (45) yet has a more expansive interface, which is shifted away from the interswitch region compared with the Arf6-specific effector JIP4 (48) and is thus less sensitive to interswitch substitutions. Additional experiments are required to delineate the remaining specificity determinants, which might include substitutions proximal to the binding interface and/or differences in isoelectric point.

The diminished ability of Arf6-GTP to stimulate 3G ARNO or 3G Cyth1 compared with 2G Grp1 derives entirely from the splice

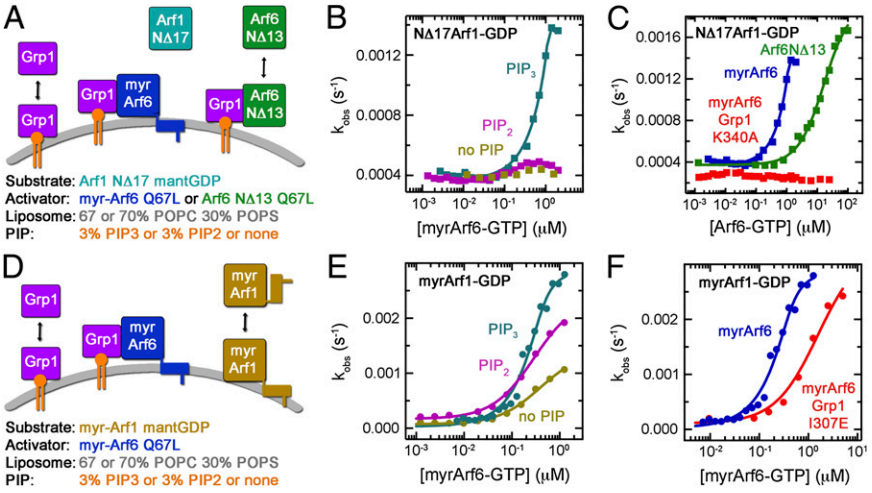

Fig. 5. Relief of autoinhibition in a membrane environment. (*A* and *D*) Schematic of protein/lipid interactions and compositions relevant to *B* and *C* (schematic in *A*) or *E* and *F* (schematic in *D*). (*B* and *C*) Catalysis of mantGDP release from 1 μM Arf1NΔ17 by 125 nM $Grp1_{63–399}$ as a function of myr-Arf6 Q67L-GppNHp. Curves are fitted quadratic models. (*C*) Catalysis of mantGDP release from 1 μM Arf1NΔ17 by 125 nM $Grp1_{63–399}$ or the K340A mutant as a function of myr-Arf6 Q67L-GppNHp or Arf6NΔ13 Q67L-GTP. (*E*) Catalysis of mantGDP release from 1 μM myr-Arf1 by 10 nM $Grp1_{63–399}$ as a function of myr-Arf6 Q67L-GTP. Curves are fitted quadratic (PIP_3) or hyperbolic models (PIP_2 and no PIP). (*F*) Catalysis of mantGDP release from 1 μM myr-Arf1 by 10 nM $Grp1_{63–399}$ or the I307E mutant as a function of myr-Arf6 Q67L-GTP. Curves are fitted quadratic models.

variation, which reduces PIP_3 affinity and, consequently, the available pool of phosphoinositide-primed precursor. Because the effective concentrations of membrane-associated cytohesins and myristoylated Arf GTPases may exceed those in the cytoplasm by several orders of magnitude, weak stimulation in solution does not exclude more robust stimulation on membranes, as observed for myr-Arf1-GTP and 3G ARNO on liposomes containing PIP_2 (37). Notably, however, relief of autoinhibition shows similar characteristics in solution and membrane environments. Indeed, the main difference lies in the concentration range of activator GTPase required to stimulate the exchange activity. Moreover, because Arf6 is expressed at lower levels than Arf1 and has a steady-state localization at the PM and on endosomes rather than the Golgi complex (49), the higher affinity for Arf6-GTP may have evolved to compensate for lower Arf6 levels. Consistent with the observation that coexpression of ARNO with either Arf1 or Arf6 promotes Arf1 recruitment to the PM (34), activation by Arf6-GTP may initiate a feedback amplification loop whereby Arf-GTP products further stimulate GEF activity (37).

Taken together, the structural and biochemical data suggest a plausible model integrating membrane targeting with allosteric activation. As depicted in Fig. 6, the 1-phosphate of the bound IP_4 can be aligned with the 1-phosphates of a simulated bilayer in an orientation optimal for simultaneous partitioning of elements known to insert into the hydrocarbon core—in particular the myristoylated N-terminal helix of Arf6-GTP and residues in the β1/β2 loop (Val-278), β3/β4 loop (Tyr-298) and βi1/βi2 hairpin (Ala-346) of the PH domain (16, 17, 50). Other elements implicated in electrostatic interactions with anionic phospholipids, including the PBR and a "sentry glutamate" that reduces basal membrane association (28, 32, 51), are located proximal to the membrane surface as are two basic residues in the β5/β6 loop (Arg-322 and Lys-323). Lateral extension of the linker suggests that the Sec7 domain may also be closer to the membrane in the Arf6–GTP complex than in the autoinhibited conformation.

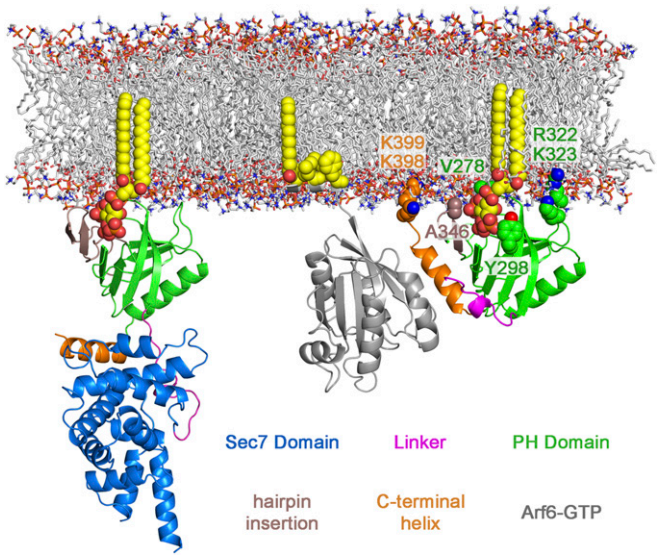

Fig. 6. Model for membrane targeting and relief of autoinhibition. (*Left*) Autoinhibited Grp1 structure (PDB ID code 2R09). (*Right*) Composite model for the active Grp1 complex with Arf6-GTP. The models are depicted in a common orientation relative to a model lipid bilayer based on the bound head group and known membrane-targeting determinants. The N-terminal helix of Arf6 is modeled in an arbitrary orientation consistent with membrane partitioning. The myristoyl and diacyl glycerol moieties are modeled in configurations compatible with membrane insertion. The POPC bilayer membrane was derived from the coordinates of a molecular dynamics simulation (61).

Autoinhibition has been observed in structurally unrelated GEFs for different GTPase families and can be relieved by various inputs, including phosphorylation and interaction with proteins or phospholipids (6, 10, 11, 52, 53). In Sos, for example, membrane association of PH and histone domains exposes an allosteric site for Ras-GTP stimulation of GEF activity (11). In cytohesins, membrane recruitment and allosteric relief of autoinhibition appear to be integrated through a unified structural mechanism whereby phosphoinositide binding primes Arf-GTP binding, which relieves autoinhibition by driving large-scale conformational rearrangements that reposition the autoinhibitory elements to reinforce membrane partitioning and support Arf substrate activation by the Sec7 domain. Given the similarity with Sos, integration of autoregulatory and membrane-targeting mechanisms in GEFs may be more prevalent than previously appreciated. Further investigation of the relationships between membrane targeting and allosteric activation will likely yield important insights into the molecular mechanisms underlying spatial–temporal–allosteric control of GTPase activation.

Materials and Methods

Myr-Arf1 was purified as described (54). Constructs and methods for expression, purification, nucleotide loading, liposome preparation, and statistical analyses are described in *SI Materials and Methods*.

Nucleotide Exchange Kinetics. Nucleotide exchange was monitored as the fluorescence decrease upon mantGDP dissociation from Arf1NΔ17 in 20 mM Tris at pH 8.0, 150 mM NaCl, 2 mM $MgCl_2$, and 250 μM or 1 mM GppNHp. Grp1 with or without active Arf GTPases, liposomes, phosphoinositides, and/or head groups was formatted into 96-well half area microplates (Corning) and incubated for 16–24 h at 25 °C. Reactions were initiated by addition of 1 μM Arf1NΔ17- or myrArf1-mantGDP and monitored by using a Safire microplate spectrophotometer (Tecan) with excitation and emission wavelengths of 360 nm and 440 nm, respectively. Observed rates constants (k_{obs}) were obtained by fitting with $I_t = (I_0 - I_\infty) \exp(-k_{obs}\, t) + I_\infty$, where I_t, I_0, and I_∞ are the emission intensities at times t, $t = 0$, and as $t \to \infty$. Catalytic efficiencies (k_{cat}/K_M) were obtained from the slope of a linear least squares fit with $k_{obs} = (k_{cat}/K_M)[GEF] + k_{intr}$, where k_{intr} is the intrinsic dissociation rate constant. Half-maximal activation constants ($K_{0.5}$) were determined by fitting with the hyperbolic function $k_{obs} = (k_\infty - k_0)\,[Arf6\text{-}GTP]/(K_{0.5} + [Arf6\text{-}GTP]) + k_0$, where k_0 and k_∞ are the values of k_{obs} at $t = 0$ and as $[Arf6\text{-}GTP] \to \infty$. For experiments in which the effective $K_{0.5}$ was comparable or less than the [GEF], the observed rate constants were fit with a quadratic function $k_{obs} = (k_\infty - k_0)\,\{b - (b^2 - 4\,[Arf6\text{-}GTP]/(n\,[GEF]))^{1/2}\} + k_0$, where $b = 1 + [Arf6\text{-}GTP]/(n\,[GEF]) + K_{0.5}/(n\,[GEF])$ and the binding stoichiometry n was fixed at 1.

Surface Plasmon Resonance. CM5 sensor chips were docked with Biacore S3000 or T100 instruments (GE Healthcare), activated, and coupled with anti-GST according to the manufacturer's instructions. Proteins were dialyzed into 20 mM Tris at pH 8.0, 150 mM NaCl, 2 mM $MgCl_2$, and 0.005% (vol/vol) P-20 surfactant. Equivalent molar quantities of GST-Grp1 constructs or GST were loaded on the sample and reference channels, respectively. Hexahistidine (6×His)-tagged Arf6-GppNHp or Arf6NΔ13 Q67L was injected for 60 s at 10 μL/min. After alignment, baseline correction, and reference subtraction, equilibrium responses (R_{eq}), which correspond to the equilibrium signal level, were determined from the average response over a 30- to 50-s range at the end of the injection. Dissociation constants (K_D) were determined by fitting with $R_{eq} = R_{max}\,[Arf6]/(K_D + [Arf6])$, where R_{max} is the value of R_{eq} as $[Arf6] \to \infty$.

Crystallization and Structure Determination. Ternary complexes were formed by incubating 6×His $Grp1_{247–399}$, 6×His Arf6NΔ13 Q67L, and IP_4 in a 1:1:1.2 molar ratio at a total concentration of 10 mg/mL for 16–18 h at 25°C. Crystals were grown by vapor diffusion from 50 mM Tris at pH 8.8, 16–18% (wt/vol) PEG 4000, and 0.2 M sodium citrate, transferred to a cryoprotectant solution (50 mM Tris at pH 8.8, 20% (wt/vol) PEG 4000, 10% (vol/vol) glycerol, and 0.2 M sodium citrate), and flash frozen in liquid nitrogen. The crystals are in the space group $P4_32_12$ with cell dimensions of $a = b =$ 56.6 Å, c = 274.4 Å and contain a single complex in the asymmetric unit. Diffraction data were collected at the Brookhaven National Synchrotron Light Source X25 beamline and processed/scaled by using HKL2000 (55). The structure was solved by molecular replacement with Phaser by using the Grp1 PH domain (1FGZ) and Arf6-GTPγS (2J5X) structures as search

models. A σA-weighted $2wF_o$-DF_c map calculated after interleaved atom updating and refinement with ARP/wWARP (56) and Refmac-5 (57) was used for automated model building with Buccaneer (58). IP_4, GTP, and solvent molecules were added by using Coot (59). The structure was refined by iterative rebuilding with Coot, atom updating with ARP/wARP, positional refinement with Refmac5, and simulated annealing with Phenix (60). Structural figures were generated by using PyMOL.

Statistical Analysis. Values and errors represent mean ± SD for two to four independent measurements.

ACKNOWLEDGMENTS. We thank Paul Randazzo for full-length human Arf6 and N-myristoyl transferase constructs as well as helpful discussion, Dr. Sean Munro for constructs of Arf3 and Arf5, and Dr. Duska Deretic for Arf4 constructs. The work was supported by National Institutes of Health Grants DK60564 and GM056324.

1. Bos JL, Rehmann H, Wittinghofer A (2007) GEFs and GAPs: Critical elements in the control of small G proteins. *Cell* 129(5):865–877.
2. Lemmon MA (2004) Pleckstrin homology domains: Not just for phosphoinositides. *Biochem Soc Trans* 32(Pt 5):707–711.
3. DiNitto JP, Lambright DG (2006) Membrane and juxtamembrane targeting by PH and PTB domains. *Biochim Biophys Acta* 1761(8):850–867.
4. Casanova JE (2007) Regulation of Arf activation: The Sec7 family of guanine nucleotide exchange factors. *Traffic* 8(11):1476–1485.
5. Donaldson JG, Jackson CL (2011) ARF family G proteins and their regulators: Roles in membrane transport, development and disease. *Nat Rev Mol Cell Biol* 12(6):362–375.
6. Sondermann H, et al. (2004) Structural analysis of autoinhibition in the Ras activator Son of sevenless. *Cell* 119(3):393–405.
7. Amor JC, et al. (2005) The structure of RalF, an ADP-ribosylation factor guanine nucleotide exchange factor from Legionella pneumophila, reveals the presence of a cap over the active site. *J Biol Chem* 280(2):1392–1400.
8. DiNitto JP, et al. (2007) Structural basis and mechanism of autoregulation in 3-phosphoinositide-dependent Grp1 family Arf GTPase exchange factors. *Mol Cell* 28(4):569–583.
9. Gureasko J, et al. (2008) Membrane-dependent signal integration by the Ras activator Son of sevenless. *Nat Struct Mol Biol* 15(5):452–461.
10. Yu B, et al. (2010) Structural and energetic mechanisms of cooperative autoinhibition and activation of Vav1. *Cell* 140(2):246–256.
11. Gureasko J, et al. (2010) Role of the histone domain in the autoinhibition and activation of the Ras activator Son of Sevenless. *Proc Natl Acad Sci USA* 107(8):3430–3435.
12. Nie Z, Hirsch DS, Randazzo PA (2003) Arf and its many interactors. *Curr Opin Cell Biol* 15(4):396–404.
13. Gillingham AK, Munro S (2007) The small G proteins of the Arf family and their regulators. *Annu Rev Cell Dev Biol* 23:579–611.
14. Franco M, Chardin P, Chabre M, Paris S (1995) Myristoylation of ADP-ribosylation factor 1 facilitates nucleotide exchange at physiological Mg2+ levels. *J Biol Chem* 270(3):1337–1341.
15. Randazzo PA, et al. (1995) The myristoylated amino terminus of ADP-ribosylation factor 1 is a phospholipid- and GTP-sensitive switch. *J Biol Chem* 270(24):14809–14815.
16. Liu Y, Kahn RA, Prestegard JH (2009) Structure and membrane interaction of myristoylated ARF1. *Structure* 17(1):79–87.
17. Liu Y, Kahn RA, Prestegard JH (2010) Dynamic structure of membrane-anchored Arf*GTP. *Nat Struct Mol Biol* 17(7):876–881.
18. Fuss B, Becker T, Zinke I, Hoch M (2006) The cytohesin Steppke is essential for insulin signalling in Drosophila. *Nature* 444(7121):945–948.
19. Hafner M, et al. (2006) Inhibition of cytohesins by SecinH3 leads to hepatic insulin resistance. *Nature* 444(7121):941–944.
20. Li J, et al. (2012) Grp1 plays a key role in linking insulin signaling to glut4 recycling. *Dev Cell* 22(6):1286–1298.
21. Kolanus W, et al. (1996) Alpha L beta 2 integrin/LFA-1 binding to ICAM-1 induced by cytohesin-1, a cytoplasmic regulatory molecule. *Cell* 86(2):233–242.
22. Chardin P, et al. (1996) A human exchange factor for ARF contains Sec7- and pleckstrin-homology domains. *Nature* 384(6608):481–484.
23. Klarlund JK, et al. (1997) Signaling by phosphoinositide-3,4,5-trisphosphate through proteins containing pleckstrin and Sec7 homology domains. *Science* 275(5308):1927–1930.
24. Rameh LE, et al. (1997) A comparative analysis of the phosphoinositide binding specificity of pleckstrin homology domains. *J Biol Chem* 272(35):22059–22066.
25. Kavran JM, et al. (1998) Specificity and promiscuity in phosphoinositide binding by pleckstrin homology domains. *J Biol Chem* 273(46):30497–30508.
26. Santy LC, Frank SR, Hatfield JC, Casanova JE (1999) Regulation of ARNO nucleotide exchange by a PH domain electrostatic switch. *Curr Biol* 9(20):1173–1176.
27. Langille SE, et al. (1999) ADP-ribosylation factor 6 as a target of guanine nucleotide exchange factor GRP1. *J Biol Chem* 274(38):27099–27104.
28. Macia E, Paris S, Chabre M (2000) Binding of the PH and polybasic C-terminal domains of ARNO to phosphoinositides and to acidic lipids. *Biochemistry* 39(19):5893–5901.
29. Klarlund JK, Tsiaras W, Holik JJ, Chawla A, Czech MP (2000) Distinct polyphosphoinositide binding selectivities for pleckstrin homology domains of GRP1-like proteins based on diglycine versus triglycine motifs. *J Biol Chem* 275(42):32816–32821.
30. Cronin TC, DiNitto JP, Czech MP, Lambright DG (2004) Structural determinants of phosphoinositide selectivity in splice variants of Grp1 family PH domains. *EMBO J* 23(19):3711–3720.
31. Venkateswarlu K, Oatey PB, Tavaré JM, Cullen PJ (1998) Insulin-dependent translocation of ARNO to the plasma membrane of adipocytes requires phosphatidylinositol 3-kinase. *Curr Biol* 8(8):463–466.
32. Nagel W, Schilcher P, Zeitlmann L, Kolanus W (1998) The PH domain and the polybasic c domain of cytohesin-1 cooperate specifically in plasma membrane association and cellular function. *Mol Biol Cell* 9(8):1981–1994.
33. Venkateswarlu K, Gunn-Moore F, Tavaré JM, Cullen PJ (1999) EGF-and NGF-stimulated translocation of cytohesin-1 to the plasma membrane of PC12 cells requires PI 3-kinase activation and a functional cytohesin-1 PH domain. *J Cell Sci* 112(Pt 12):1957–1965.
34. Cohen LA, et al. (2007) Active Arf6 recruits ARNO/cytohesin GEFs to the PM by binding their PH domains. *Mol Biol Cell* 18(6):2244–2253.
35. Hofmann I, Thompson A, Sanderson CM, Munro S (2007) The Arl4 family of small G proteins can recruit the cytohesin Arf6 exchange factors to the plasma membrane. *Curr Biol* 17(8):711–716.
36. Li CC, et al. (2007) ARL4D recruits cytohesin-2/ARNO to modulate actin remodeling. *Mol Biol Cell* 18(11):4420–4437.
37. Stalder D, et al. (2011) Kinetic studies of the Arf activator Arno on model membranes in the presence of Arf effectors suggest control by a positive feedback loop. *J Biol Chem* 286(5):3873–3883.
38. Goldberg J (1998) Structural basis for activation of ARF GTPase: Mechanisms of guanine nucleotide exchange and GTP-myristoyl switching. *Cell* 95(2):237–248.
39. Ferguson KM, et al. (2000) Structural basis for discrimination of 3-phosphoinositides by pleckstrin homology domains. *Mol Cell* 6(2):373–384.
40. Lietzke SE, et al. (2000) Structural basis of 3-phosphoinositide recognition by pleckstrin homology domains. *Mol Cell* 6(2):385–394.
41. Renault L, Guibert B, Cherfils J (2003) Structural snapshots of the mechanism and inhibition of a guanine nucleotide exchange factor. *Nature* 426(6966):525–530.
42. Mossessova E, Corpina RA, Goldberg J (2003) Crystal structure of ARF1*Sec7 complexed with Brefeldin A and its implications for the guanine nucleotide exchange mechanism. *Mol Cell* 12(6):1403–1411.
43. He J, et al. (2008) Molecular mechanism of membrane targeting by the GRP1 PH domain. *J Lipid Res* 49(8):1807–1815.
44. Pasqualato S, Ménétrey J, Franco M, Cherfils J (2001) The structural GDP/GTP cycle of human Arf6. *EMBO Rep* 2(3):234–238.
45. Chavrier P, Ménétrey J (2010) Toward a structural understanding of arf family:effector specificity. *Structure* 18(12):1552–1558.
46. Ménétrey J, et al. (2007) Structural basis for ARF1-mediated recruitment of ARHGAP21 to Golgi membranes. *EMBO J* 26(7):1953–1962.
47. Várnai P, et al. (2005) Selective cellular effects of overexpressed pleckstrin-homology domains that recognize PtdIns(3,4,5)P3 suggest their interaction with protein binding partners. *J Cell Sci* 118(Pt 20):4879–4888.
48. Isabet T, et al. (2009) The structural basis of Arf effector specificity: The crystal structure of ARF6 in a complex with JIP4. *EMBO J* 28(18):2835–2845.
49. Cavenagh MM, et al. (1996) Intracellular distribution of Arf proteins in mammalian cells. Arf6 is uniquely localized to the plasma membrane. *J Biol Chem* 271(36):21767–21774.
50. Lumb CN, et al. (2011) Biophysical and computational studies of membrane penetration by the GRP1 pleckstrin homology domain. *Structure* 19(9):1338–1346.
51. Pilling C, Landgraf KE, Falke JJ (2011) The GRP1 PH domain, like the AKT1 PH domain, possesses a sentry glutamate residue essential for specific targeting to plasma membrane PI(3,4,5)P(3). *Biochemistry* 50(45):9845–9856.
52. Freedman TS, et al. (2006) A Ras-induced conformational switch in the Ras activator Son of sevenless. *Proc Natl Acad Sci USA* 103(45):16692–16697.
53. Aghazadeh B, Lowry WE, Huang XY, Rosen MK (2000) Structural basis for relief of autoinhibition of the Dbl homology domain of proto-oncogene Vav by tyrosine phosphorylation. *Cell* 102(5):625–633.
54. Luo R, et al. (2007) Kinetic analysis of GTP hydrolysis catalysed by the Arf1-GTP-ASAP1 complex. *Biochem J* 402(3):439–447.
55. Otwinowski Z, Minor W (1997) Processing of x-ray diffraction data collected in oscillation mode. *Methods in Enzymology*, eds Carter CW Jr., Sweet RM (Academic, New York) Vol 276, Part A, 307–326.
56. Langer G, Cohen SX, Lamzin VS, Perrakis A (2008) Automated macromolecular model building for X-ray crystallography using ARP/wARP version 7. *Nat Protoc* 3(7):1171–1179.
57. Murshudov GN, et al. (2011) REFMAC5 for the refinement of macromolecular crystal structures. *Acta Crystallogr D Biol Crystallogr* 67(Pt 4):355–367.
58. Cowtan K (2006) The Buccaneer software for automated model building. 1. Tracing protein chains. *Acta Crystallogr D Biol Crystallogr* 62(Pt 9):1002–1011.
59. Emsley P, Lohkamp B, Scott WG, Cowtan K (2010) Features and development of Coot. *Acta Crystallogr D Biol Crystallogr* 66(Pt 4):486–501.
60. Adams PD, et al. (2010) PHENIX: A comprehensive Python-based system for macromolecular structure solution. *Acta Crystallogr D Biol Crystallogr* 66(Pt 2):213–221.
61. Heller H, Schaefer M, Schulten K (1993) Molecular dynamics simulation of a bilayer of 200 lipids in the gel and in the liquid-crystal phases. *J Phys Chem* 97:8343–8360.